Proceedings of the 2nd International Conference on Robotics,
Computer Vision and Intelligent Systems - ROBOVIS, 27-20 October, Virtual Event
https://www.insticc.org/node/TechnicalProgram/ROBOVIS/2021/presentationDetails/107121

On-orbit free-floating manipulation using a two-arm robotic system

Jose Luis Ramon[1][a], Jorge Pomares[1][b] and Leonard Felicetti[2][c]
[1]*University of Alicante, Department of Physics, Systems Engineering and Signal Theory, Alicante, Spain*
[2]*Cranfield University, School of Aerospace, Transport and Manufacturing, Cranfield, United Kingdom*
jl.ramon@ua.es, jpomares@ua.es, leonard.felicetti@cranfield.ac.uk

Keywords: Dual-Arm Manipulator; Space Robotics; On-Orbit Servicing; Visual Servoing; Impedance Control.

Abstract: A direct visual-servoing algorithm is proposed for the control of a space-based two-arm manipulator. The scenario under consideration assumes that one of the arms performs the manipulation task while the second one has an in-hand camera to observe the target zone of manipulation. The algorithm uses both the camera images and the force/torque measurements as inputs to calculate the control action to move the arms to perform a manipulation task. The algorithm integrates the multibody dynamics of the robotic system in a visual servoing framework that uses de-localized cameras. Impedance control is then used to compensate for eventual contact reactions when the end effector touches and operates the target body. Numerical results demonstrate the suitability of the proposed algorithm in specific tasks used in on-orbit servicing operations.

1 INTRODUCTION

Space manipulators will be used in a growing range of missions to assemble, repair, resupply, and rescue satellites in orbit or remove them at the end of life (Flores-Abad et al.,2014). Rigorous requirements in terms of accuracy and safety of the robotic operations are generally imposed in such kinds of applications, as it is imperative to avoid collisions that can damage equipment or compromise the success of missions (Felicetti et al., 2016). These tasks become even more challenging when targets are in uncontrolled non-cooperative conditions (Moghaddam & Chhabra, 2021) or the servicing spacecraft is maintained in a free-floating condition (Xu et al., 2020).

In such kinds of robotic operations, the knowledge of the relative position between the service spacecraft and the target must be continuously monitored to avoid collisions (Cassinis et al., 2019). Onboard cameras are preferred over all other sensors, as they have higher technology readiness levels, a higher degree of reliability, and better versatility than other solutions (Palmerini et al., 2016). Cameras can be located on the main body of the servicing spacecraft or on movable and reconfigurable appendages to avoid occlusions of the observed scene during the manipulation task (Peng et al., 2021) (Wang et al., 2017).

This paper focuses on the specific scenario where a servicing spacecraft equipped with robotic arms performs on-orbit servicing and manipulation operations. Specifically, the spacecraft is assumed to be equipped with two robotic arms serving the manipulation and observation functions, respectively. The first manipulator is an anthropomorphic robotic arm with all the useful tools to grasp and manipulate parts of the target satellite. The second manipulator is a robotic arm with an eye-in-hand camera system used to observe the specific target area where the robotic operations are performed. In addition, in order to better perform the manipulator task, it is necessary to have also knowledge of the contact forces and torques with the targets. For this reason, the scenario assumes that force sensors at the end-effector are able to measure these actions (Garcia et al., 2019).

This paper proposes a new approach to build a visual servoing controller that considers the relative free-floating condition of the bodies involved in the operations and integrates it with an impedance control strategy for compensating eventual contact reactions

[a] https://orcid.org/0000-0002-8635-6061
[b] https://orcid.org/0000-0002-7523-9118
[c] https://orcid.org/0000-0001-6830-4308

Published by Scitepress. This is the Author Accepted Manuscript issued with:
Creative Commons Attribution Non-Commercial No Derivatives License (CC:BY:NC:ND 4.0).
Please refer to any applicable publisher terms of use.

during the manipulation. Visual servoing is a well-known approach to guide robots using visual information obtained from cameras (Chaumette & Hutchinson, 2006). Image-based visual servoing systems allow for the robot guidance by only using image information and do not require reconstructing the 3D position of the target to guide the robot. The proposed controller assumes that the target trajectory is defined directly in the image space, and it calculates the torques to be applied to the manipulator's joints to perform the manipulation task. The proposed direct image-based visual servoing control outputs the joint torques directly, without having internal control loops of servo motors. This characteristic offers advantages in the guidance of space robots: eventual actions on the main servicing spacecraft body can be easily computed and predicted. In (Alepuz et al., 2016), a direct image-based controller is proposed for the guidance of a free-floating manipulator using an eye-in-hand camera. In (Pomares et al., 2018), a visual servoing system is proposed to guide a spacecraft during a rendezvous manoeuvre. In this case, a camera is attached to the servicing spacecraft. The approach presented in this paper assumes that the camera is moving alongside the second arm. Consequently, control actions are generated independently of the unknown position of the camera. The second arm can be moved to ensure better views of the observed scene of manipulation.

The proposed visual servoing algorithm also integrates force and torque measurements at the manipulator end effector to increase the system robustness when interacting with the target body. A mix between a visual servoing controller and impedance control is proposed in (Garcia et al., 2020) to perform spacecraft docking in on-orbit servicing operations. Impedance control is also used in (Mitros et al., 2017) to evaluate and compensate the interface contact actions during on-orbit docking manoeuvres between two spacecraft. A servicing spacecraft with a force-controlled manipulation system is also presented in (Dalyaev et al., 2018), using an impedance control to touch and move the end effector over the target surface. In on-orbit servicing applications, the relative dynamics and eventual contact dynamics between the target and the servicing spacecraft might strongly affect the performance of the robotic operations. In such circumstances, indirect approaches are preferable over direct ones. This is the case of the algorithms proposed in (Garcia et al., 2019) (Garcia et al., 2020), where the impedance controller is paired with a vision control to help keep the manipulator aligned during the manipulation tasks. The algorithm presented in this paper proposes an image-based visual impedance control law that simultaneously combines the inputs from the camera and the force sensors. Simulation results will show that the use of such a controller allows for an increase of tracking precision with respect to the previous direct visual servoing approaches. To validate the methodology, this paper shows the results of an insertion task. The proposed controllers can compensate for the tool's eventual misalignments while this is inserted in a hole in the target spacecraft.

The remaining part of the paper is organized as follows: Section 2 describes the system architecture proposed for the servicing spacecraft and its dynamics. The visual servoing and interaction control are described in Section 3 and Section 4, respectively. Section 5 presents the numerical results used to assess the controllers' validity and robustness on the trajectory tracking and the tool insertion tasks. Finally, Section 6 summarizes the main findings and presents the concluding remarks.

2 SYSTEM ARCHITECTURE

2.1 On-orbit servicing scenario

A representation of the on-orbit servicing scenario is shown in Figure 1. A servicing spacecraft is supposed to perform some on-orbit servicing operations to a target spacecraft. The servicing spacecraft is equipped with two robotics arms that serve two functions: manipulation and observation, respectively. The first manipulator has ne rotational joints and it is used for accomplishing the manipulation tasks. The second manipulator is a robotic arm with nc degrees of freedom with an eye-in-hand camera system.

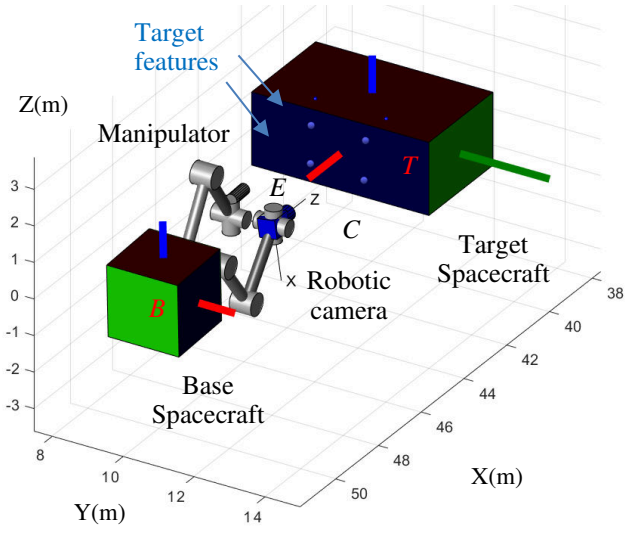


Figure 1 On-orbit servicing scenario

A pattern with m points is attached to the target spacecraft. The robotic camera will use this to identify the relative pose of the target spacecraft.

Figure 1 also shows the coordinate frames adopted in this study. The *B* frame is attached to the servicing spacecraft's main body, and the *T* frame is used for the target spacecraft. Two other coordinate frames represent the pose of the end-effectors of both the robotic arms: the *C* frame at the eye-in-hand camera and the *E* frame at the end of the manipulator's arm. Finally, an Earth Centered Inertial coordinate frame, called *I*, is adopted as a reference frame for calculating the objects' positions and attitudes included in the scenario.

2.2 System dynamics

The current configuration of the servicing spacecraft and its two robotic arms is represented by the state vector $\boldsymbol{\epsilon} = \left[\boldsymbol{t}_b^{I\,T}, \boldsymbol{\phi}_b^{I\,T}, \boldsymbol{q}_e^T, \boldsymbol{q}_c^T\right]^T$, where $\boldsymbol{t}_b^I$ and $\boldsymbol{\phi}_b^I$ are the position vector and attitude coordinates (Euler angles) of the base spacecraft with respect to the Inertial frame and, $\boldsymbol{q}_e^T$ and $\boldsymbol{q}_c^T$ are the joint angles of both the manipulator and the robotic camera, respectively.

The equation of motion of robotic system can be written as (Pisculli et al., 2014):

$$\begin{bmatrix} \boldsymbol{h}_b^I \\ \boldsymbol{\tau}_e \\ \boldsymbol{\tau}_c \end{bmatrix} = \begin{bmatrix} \boldsymbol{M}_{bb} & \boldsymbol{M}_{be} & \boldsymbol{M}_{bc} \\ \boldsymbol{M}_{be}^T & \boldsymbol{M}_{ee} & 0 \\ \boldsymbol{M}_{bc}^T & 0 & \boldsymbol{M}_{cc} \end{bmatrix} \begin{bmatrix} \dot{\boldsymbol{v}}_b^I \\ \ddot{\boldsymbol{q}}_e \\ \ddot{\boldsymbol{q}}_c \end{bmatrix} + \begin{bmatrix} \boldsymbol{c}_b \\ \boldsymbol{c}_e \\ \boldsymbol{c}_c \end{bmatrix} + \boldsymbol{J}^T \begin{bmatrix} \boldsymbol{0}_6 \\ \boldsymbol{h}_e^I \\ \boldsymbol{0}_6 \end{bmatrix} \quad (1)$$

where $\ddot{\boldsymbol{q}}_e$ and $\ddot{\boldsymbol{q}}_c$ is the set of joint accelerations of the robot manipulator and camera, respectively, $\dot{\boldsymbol{v}}_b^I = \left[\ddot{\boldsymbol{t}}_b^{I\,T}, \dot{\boldsymbol{\omega}}_b^{I\,T}\right]^T \in \Re^6$ denotes the linear and angular accelerations of the base spacecraft expressed in the Inertial coordinate frame, $\boldsymbol{M}_{bb} \in \Re^{6\times6}$ is the inertia matrix of the base spacecraft, $\boldsymbol{M}_{be} \in \Re^{6\times ne}$ is the coupling matrix between the spacecraft and the manipulator, $\boldsymbol{M}_{ee} \in \Re^{ne\times ne}$ is the inertia matrix of the manipulator, $\boldsymbol{M}_{bc} \in \Re^{6\times nc}$ is the coupling matrix between the spacecraft and the robotic camera, $\boldsymbol{M}_{cc} \in \Re^{nc\times nc}$ is the inertia matrix of the robotic camera; $\boldsymbol{c}_b$, $\boldsymbol{c}_e$, and $\boldsymbol{c}_c \in \Re^6$ are a velocity/displacement-dependent, non-linear terms for the base, manipulator and robotic camera, respectively, $\boldsymbol{h}_b^I \in \Re^6$ includes both the force and torque exerted on the base of the servicing spacecraft but in this paper no forces and torques will be applied to the servicing spacecraft, $\boldsymbol{\tau}_e \in \Re^{ne}$ and $\boldsymbol{\tau}_c \in \Re^{nc}$ are the applied set of joint torques acting on the robot manipulator and on the robotic camera, respectively. It is also worth noting that eventual external wrenches $\boldsymbol{h}_e^I$ on the end effector can be projected into the joint space by using the Jacobian $\boldsymbol{J}^T$ and therefore can be included into the robot dynamics.

3 VISUAL SERVOING

The proposed visual-based control uses features of the target body for driving both the robotic manipulator and the robotic camera. Figure 1 shows a pattern of m points attached on the body of the target satellite that might represent possible visual features observed by the robotic camera. These points have fixed positions with respect to the target coordinate frame ($\boldsymbol{p}_{t,i}^T = \begin{bmatrix} x_{t,i}^T & y_{t,i}^T & z_{t,i}^T \end{bmatrix}$, with $i = 1 \dots m$), but they will appear as 2D points in the camera image plane $\boldsymbol{s}_{t,i} = \left[X_{t,i}, Y_{t,i}\right]^T \in \Re^2$, after being projected through a pin-hole camera model (Ma et al., 2015). The controller is built upon the concept that the same set of m features seen in the target can be virtually generated and attached to the manipulator's end effector and therefore moving rigidly with it.

The visual-servoing controller aims to match the virtual features with ones attached to the target. In this way, the robotic manipulator follows a specified trajectory defined in the image plane of the robotic camera. Thus, the position of each of the virtual features, $\boldsymbol{p}_{e,i}^E$, with $i = 1 \dots m$, will be considered constant with respect to the coordinate frame of the end-effector. The corresponding virtual image features, $\boldsymbol{s}_{e,i} = \left[X_{e,i}, Y_{e,i}\right]^T \in \Re^2$, are obtained taking into account the manipulator kinematics. The camera position is known from the actual arm configuration; therefore, it is possible to relate the manipulator end-effector position with the position of the robotic camera through an algebraic relation given by the direct kinematics of the two manipulators. A pin-hole camera model is then used for projecting each of the points in the camera frame $\boldsymbol{p}_{e,i}^C = \left[x_{e,i}^C, y_{e,i}^C, z_{e,i}^C\right]^T$ onto the image plane, $\boldsymbol{s}_{e,i} = \left[X_{e,i}, Y_{e,i}\right]^T$, using the following equation:

$$\boldsymbol{s}_{e,i} = \frac{1}{z_{e,i}^C} \begin{bmatrix} x_{e,i}^C \\ y_{e,i}^C \end{bmatrix} \quad (2)$$

where $\boldsymbol{p}_{e,i}^C = \left[x_{e,i}^C, y_{e,i}^C, z_{e,i}^C\right]^T \in \Re^3$ is the position of the i-th point with respect the camera frame. The time derivative of the virtual features are:

$$\dot{\boldsymbol{s}}_{e,i} = \left[\dot{X}_{e,i}, \dot{Y}_{e,i}\right]^t = \boldsymbol{L}_{e,i} \dot{\boldsymbol{p}}_{e,i}^C \quad (3)$$

with:

$$\boldsymbol{L}_{e,i} = \frac{1}{z_{e,i}^C} \begin{bmatrix} 1 & 0 & -X_{e,i} \\ 0 & 1 & -Y_{e,i} \end{bmatrix} \quad (4)$$

The value of $\dot{\boldsymbol{p}}_{e,i}^{C}$ can be obtained from $\boldsymbol{p}_{e,i}^{E}$ taking into account the relationship between both frames:

$$\dot{\boldsymbol{p}}_{e,i}^{C} = \begin{bmatrix} \boldsymbol{E}_3 & -sk\left(\boldsymbol{R}_E^C \boldsymbol{p}_{e,i}^E\right) \end{bmatrix} \begin{bmatrix} \boldsymbol{R}_C^I & \boldsymbol{0}_{3x3} \\ \boldsymbol{0}_{3x3} & \boldsymbol{R}_C^I \end{bmatrix}^T \cdot \cdot \left(\boldsymbol{v}_e^I - \boldsymbol{v}_c^I\right) \quad (5)$$

where $\boldsymbol{R}_c^I$ is the rotation matrix between the camera and the Inertial frame, $\boldsymbol{v}_e^I$ and $\boldsymbol{v}_c^I$ are the twist of the end-effector, *E*, and the camera, *C*, with respect the Inertial frame, and $\boldsymbol{E}_3 \in \Re^{3x3}$ the identity matrix. Finally, the Jacobian matrix $\boldsymbol{J}_{e,i}$ can be defined as:

$$\begin{aligned} &\dot{\boldsymbol{s}}_{e,i} = \\ &= \boldsymbol{L}_{e,i}\begin{bmatrix} \boldsymbol{E}_3 & -sk\left(\boldsymbol{R}_E^C \boldsymbol{p}_{e,i}^E\right) \end{bmatrix} \begin{bmatrix} \boldsymbol{R}_C^I & \boldsymbol{0}_{3x3} \\ \boldsymbol{0}_{3x3} & \boldsymbol{R}_C^I \end{bmatrix}^T \\ &\left(\boldsymbol{v}_e^I - \boldsymbol{v}_c^I\right) = \boldsymbol{J}_{e,i}\left(\boldsymbol{v}_e^I - \boldsymbol{v}_c^I\right) \end{aligned} \quad (6)$$

On the other hand, the time derivative of the visual features extracted from the target spacecraft (using the robotic camera) can be obtained using the interaction matrix, $\boldsymbol{L}_{t,i}$, used in classical image-based visual servoing systems (Ma et al., 2015):

$$\boldsymbol{L}_{t,i} = \begin{bmatrix} -\frac{1}{z_{t,i}^C} & 0 & \frac{X_{t,i}}{z_{t,i}^C} \\ 0 & -\frac{1}{z_{t,i}^C} & \frac{Y_{t,i}}{z_{t,i}^C} \\ X_{t,i}Y_{t,i} & -1 - X_{t,i}^2 & Y_{t,i} \\ 1 + Y_{t,i}^2 & -X_{t,i}Y_{t,i} & -X_{t,i} \end{bmatrix} \quad (7)$$

Therefore:

$$\begin{aligned} \dot{\boldsymbol{s}}_{t,i} = \left[\dot{X}_{t,i}, \dot{Y}_{t,i}\right]^T &= \boldsymbol{L}_{t,i} \begin{bmatrix} \boldsymbol{R}_C^I & \boldsymbol{0}_{3x3} \\ \boldsymbol{0}_{3x3} & \boldsymbol{R}_C^I \end{bmatrix}^T \boldsymbol{v}_c^I \\ &= \boldsymbol{J}_{t,i}\boldsymbol{v}_c^I \end{aligned} \quad (8)$$

The aim of the visual-servoing controller is to reduce the image error $\boldsymbol{e}_s = \boldsymbol{s}_e - \boldsymbol{s}_t$ to zero, where $\boldsymbol{s}_e = [\boldsymbol{s}_{e1}, \boldsymbol{s}_{e2}, \dots, \boldsymbol{s}_{em}]^T$ and $\boldsymbol{s}_t = [\boldsymbol{s}_{t1}, \boldsymbol{s}_{t2}, \dots, \boldsymbol{s}_{tm}]^T$ are the virtual features and the real ones extracted by the robotic camera, respectively.

4 INTERACTION CONTROL

The proposed control scheme takes the contact dynamics between the two bodies into account to compensate for eventual reactions and disturbances produced during the contact. This study assumes that the target spacecraft has a greater mass than the servicing spacecraft so that the target's motion does not change significantly due to the interaction with the servicer's end-effector. On the other hand, reaction forces produced by the contact dynamics can produce significant changes in both the position and attitude dynamics of the servicing spacecraft.

A damper-spring model is used in this paper to characterize this kind of interaction. Therefore, the visual servoing approach generates a virtual damper-spring behaviour for the pose displacement generated by the visual error (Tommasino et al., 2020):

$$\boldsymbol{D}\boldsymbol{v}_{ed}^I + \boldsymbol{\alpha} = \boldsymbol{h}_e^I \quad (9)$$

where $\boldsymbol{D}$ is the damping matrix, $\boldsymbol{v}_{ed}^I$ is the desired twist of the manipulator-end and includes both linear and angular velocities, $\boldsymbol{h}_e^I \in \Re^6$ is the external wrench action on the manipulator and $\boldsymbol{\alpha} \in \Re^6$ is the control law to be defined for the visual servoing task. The following Lyapunov function is considered:

$$\boldsymbol{V}(\boldsymbol{e}_s) = \frac{1}{2}\boldsymbol{e}_s^T\boldsymbol{Q}\boldsymbol{e}_s \quad (10)$$

where $\boldsymbol{Q}$ is a diagonal positive definite matrix to guarantee the system stability. The time derivative of the previous Lyapunov function is:

$$\dot{\boldsymbol{V}}(\boldsymbol{e}_s) = \boldsymbol{e}_s^T\boldsymbol{Q}\dot{\boldsymbol{e}}_s \quad (11)$$

By using Eq. (6) and (8), the time derivative of the image error can be calculated as:

$$\begin{aligned} \dot{\boldsymbol{e}}_s = \dot{\boldsymbol{s}}_e - \dot{\boldsymbol{s}}_t &= \boldsymbol{J}_e\left(\boldsymbol{v}_{ed}^I - \boldsymbol{v}_c^I\right) - \boldsymbol{J}_t\boldsymbol{v}_c^I \\ &= \boldsymbol{J}_e\boldsymbol{v}_{ed}^I \\ &\quad - \left(\boldsymbol{J}_t + \boldsymbol{J}_e\right)\boldsymbol{v}_c^I \\ &= \boldsymbol{J}_e\boldsymbol{v}_{ed}^I - \boldsymbol{J}_c\boldsymbol{v}_c^I \end{aligned} \quad (12)$$

where $\boldsymbol{J}_e = \left[\boldsymbol{J}_{e,1}^T, \boldsymbol{J}_{e,2}^T, \dots, \boldsymbol{J}_{e,m}^T\right]^T \in \Re^{2mx6}$, $\boldsymbol{J}_t = \left[\boldsymbol{J}_{t,1}^T, \boldsymbol{J}_{t,2}^T, \dots, \boldsymbol{J}_{t,m}^T\right]^T \in \Re^{2mx6}$ and $\boldsymbol{J}_c = \boldsymbol{J}_t + \boldsymbol{J}_e$.

Thus, by taking into account Eq.(12) and (9), the value of $\dot{\boldsymbol{V}}$ becomes:

$$\begin{aligned} \dot{\boldsymbol{V}}(\boldsymbol{e}_s) &= \boldsymbol{e}_s^T\boldsymbol{Q}\left(\boldsymbol{J}_e\boldsymbol{v}_{ed}^I - \boldsymbol{J}_c\boldsymbol{v}_c^I\right) \\ &= \boldsymbol{e}_s^T\boldsymbol{Q}\left(\boldsymbol{J}_e\boldsymbol{D}^{-1}\left(\boldsymbol{h}_e^I\right.\right. \\ &\quad \left.\left. - \boldsymbol{\alpha}\right) - \boldsymbol{J}_c\boldsymbol{v}_c^I\right) \end{aligned} \quad (13)$$

and, if we consider the following control action:

$$\boldsymbol{\alpha} = \boldsymbol{D}\left(\boldsymbol{K}\boldsymbol{J}_e^+\boldsymbol{Q}\boldsymbol{e}_s - \boldsymbol{J}_e^+\boldsymbol{J}_c\boldsymbol{v}_c^I\right) \quad (14)$$

being $\boldsymbol{K}$ a positive definite matrix, Eq. (13) becomes:

$$\begin{aligned} \dot{\boldsymbol{V}}(\boldsymbol{e}_s) &= \boldsymbol{e}_s^T\boldsymbol{Q}\boldsymbol{J}_e\boldsymbol{D}^{-1}\boldsymbol{h}_e^I \\ &\quad - \boldsymbol{e}_s^T\boldsymbol{Q}\boldsymbol{J}_e\boldsymbol{K}\boldsymbol{J}_e^+\boldsymbol{Q}\boldsymbol{e}_s \end{aligned} \quad (15)$$

It is worth noting that, when the robot does not interact with the target spacecraft, there are no external actions acting on the end-effector ($\boldsymbol{h}_e^I = 0$), therefore $\dot{\boldsymbol{V}}(\boldsymbol{e}_s) = -\boldsymbol{e}_s^T\boldsymbol{Q}\boldsymbol{J}_e\boldsymbol{K}\boldsymbol{J}_e^+\boldsymbol{Q}\boldsymbol{e}_s$ and consequently, the system in Eq.(9) is asymptotically

stable: the reference trajectory tracking task will be achieved at the equilibrium $\boldsymbol{e}_s = 0$ if $\boldsymbol{J}_e$ is nonsingular. On the other hand, when the robot interacts with the target spacecraft, Eq. (9) can be used in conjunction with Eq.(14) to obtain:

$$\boldsymbol{D}\boldsymbol{v}_{ed}^{I} + \boldsymbol{D}\boldsymbol{K}(\boldsymbol{J}_e^{+}\boldsymbol{Q}\boldsymbol{e}_s - \boldsymbol{K}^{-1}\boldsymbol{J}_e^{+}\boldsymbol{J}_c\boldsymbol{v}_c^{I}) = \boldsymbol{h}_e^{I} \quad (16)$$

The desired interaction compliance can be defined in the Cartesian space by means of the matrices $\boldsymbol{K}$ and $\boldsymbol{D}$ and the image convergence can be regulated by setting selected gains for $\boldsymbol{Q}$. Specifically, this is done by formulating an optimal control strategy for tracking the reference trajectory obtained from the interaction wrench and the image error. This tracker has been developed in (Pomares et al., 2015).

5 RESULTS

Simulations have been carried on to assess the performance of the proposed visual-servoing control strategy when performing the task of tool insertion into the body of the target spacecraft. A predefined trajectory is followed by the robotic camera. This trajectory is pre-planned offline so that the visual features remain within the field of view during the task. The control of the robot camera trajectory is out of the scope of this study, but approaches like the ones shown in (Garcia et al., 2020) (Mitros et al., 2017) can guarantee that the camera can correctly observe the areas of interest for performing the operations.

The mass properties of the manipulator, of the robotic camera and of the base satellite are listed in Table 1. The controller matrices are set as follows:

$$\boldsymbol{Q} = diag(0.01) \in \Re^{2m\times 2m},$$
$$\boldsymbol{K} = diag(0.1, 0.1, 0.4, 10, 10, 15),$$
$$\boldsymbol{D} = diag(100, 100, 400, 10, 10, 20),$$

where $diag(\,)$ is a matrix with the diagonal elements equal to the argument of the function. The camera acquires 20 images per second with a resolution of 640x480 pixels but the control loop is running at 5 ms. The camera is supposed to be previously calibrated and the intrinsic parameters are (u_0, v_0) = (298, 225) px, and (f_u, f_v) = (1082.3, 1073.7) px, where u_0 and v_0 are the position of the optical center and f_u and f_v are the focal lengths in the x and y directions, respectively. A tool is held by the robotic manipulator end-effector and needs to inserted 2 cm into the target spacecraft.

An offset of 3 mm from the ideal configuration of the virtual features is included in the desired pattern to simulate an error in the final pose. In this way, it is possible to evaluate the effectiveness of the proposed control scheme to guide the robotic manipulator in the presence of contact forces: some adjustments will be needed by the embedded impedance control.

TABLE I. DYNAMIC PARAMETERS OF THE ROBOT

	Mass (Kg)	Inertia (kg·m²)		
Base		I_x	I_y	I_z
	2550	6200	3540	7090
Arms	**Mass (Kg)**	**Inertia (kg·m²)**		
		I_x	I_y	I_z
	2550	6200	3540	7090
Link1	35	2	0.2	2
Link2	22	3	0.2	3
Link3	22	3	0.2	3
Link4	10	0.15	0.2	0.4
Link5	10	0.15	0.2	0.3
Link6	10	0.2	0.25	0.3

The simulation results are shown from Figure 2 to Figure 4. Specifically, the 3D trajectory described by the robotic system is shown in Figure 2, where the trajectory of the manipulator is highligthed in red and the trajectory of the robotic camera in blue. From the overlapping frames, it is possible to evaluate the movements of the manipulator, which tries to extend its arm to reach the target. At the same time, the floating base of the satellite moves backwards as a reaction to the motion of both manipulator and robotic camera.

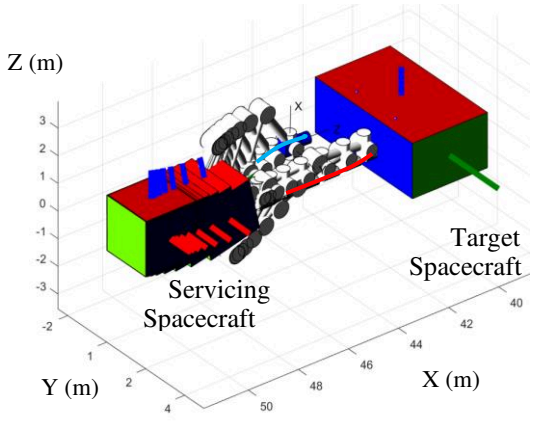


Figure 2 Robot arm trajcetories during the tool insertion task

The corresponding motion of the image features in the image plane is shown in Figure 3. The trajectories of the visual features extracted from the target spacecraft are represented in blue, and the trajectories of the virtual features are shown in red. Empty circles and the final features indicate the initial features are shown by solid circles.

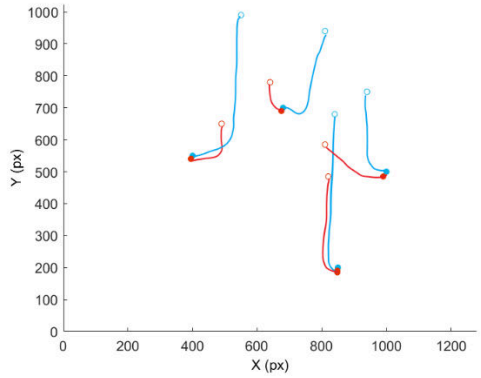


Figure 3 Image trajectories of the virtual and real visual features

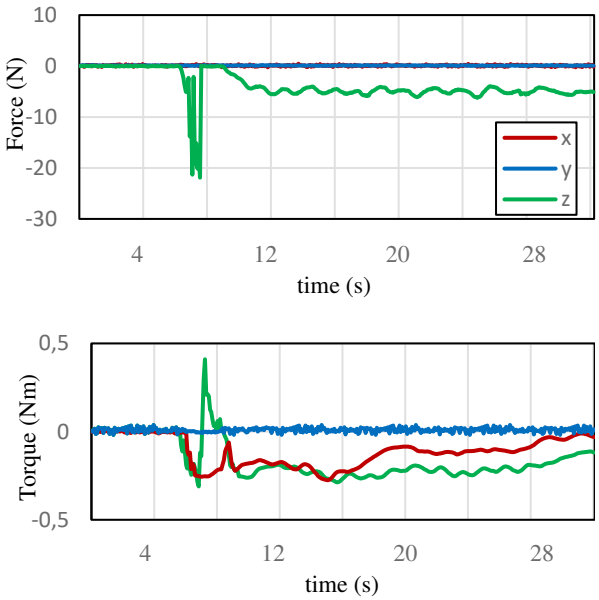


Figure 4 Reaction forces and torques during the insertion task

As expected, the positions of the extracted image features and virtual features are initially very far from each other, but they tend to approach each other during the manoeuvre. However, their final position in the image plane is not perfectly matching due to the offset between the actual virtual target configuration and the ideal one. The controller, in any case, compensates for this error by using the impedance strategy shown in Section 4. The time behaviour of the reaction forces and torques at the end effector of the manipulator are shown in Figure 4. The peak of the contact forces is reached after 7 s, when the tool touches the target for the first time but cannot be correctly inserted in the first attempt. After this initial phase, the offset on the virtual target image is compensated within the controller. The contact forces reduce their values when the tool is centred and inserted into the hole.

6 CONCLUSIONS

The paper presented a direct visual servoing algorithm suitable for on-orbit servicing and manipulation. The algorithm is applicable to a spacecraft equipped with two-arm manipulator. The two arms are dedicated to manipulation and observation tasks, respectively.

A visual servoing controller independent from the observed scene's point of view was consequently developed. The virtual features could be virtually reconstructed following a specific pattern seen on the target body and consequently assumed attached to the end effector of the operating manipulator.

The controller was able to drive the manipulator in such a way to make the virtual features match the real features on the target body. Under an impedance control scheme, the controller also compensated for eventual contact reactions between the end effector and the target satellite. Simulations demonstrated the applicability of this scheme in a standard multi-degrees of freedom manipulator scenario where eventual misalignments that would not allow for a tool insertion task inside the body of the target satellite were compensated and corrected by the controller, making this kind of operation still successful.

Further studies will assess the robustness of the proposed controller against environmental torques and forces as well as will evaluate the performance of the controller with different frame rates of the camera, and will compare the results with other tracking controllers.

REFERENCES

Alepuz, J. P., Emami, M. R., & Pomares, J. (2016). Direct image-based visual servoing of free-floating space manipulators. Aerospace Science and Technology, 55, 1–9. https://doi.org/10.1016/j.ast.2016.05.012.

Cassinis, L. P., Fonod, R., & Gill, E. (2019). Review of the robustness and applicability of monocular pose estimation systems for relative navigation with an uncooperative spacecraft. Progress in Aerospace Sciences, 110, 008.

Chaumette, F., & Hutchinson, S. (2006). Visual servo control. I. Basic approaches. IEEE Robotics & Automation Magazine, 13(4), 82–90. https://doi.org/10.1109/MRA.2006.250573.

Dalyaev, I., Titov, V., & Shardyko, I. (2018). A concept of robotic system with force-controlled manipulators for on-orbit servicing spacecraft. En Proceedings of the Scientific-Practical Conference «Research and Development - 2016» (pp. 239-245). Springer International Publishing.

Felicetti, L., Gasbarri, P., Pisculli, A., Sabatini, M., & Palmerini, G. B. (2016). Design of robotic manipulators for orbit removal of spent launchers' stages. Acta Astronautica, 119, 118–130. https://doi.org/10.1016/j.actaastro.2015.11.012.

Flores-Abad, A., Ma, O., Pham, K., & Ulrich, S. (2014). A review of space robotics technologies for on-orbit servicing. Progress in Aerospace Sciences, 68, 1–26. https://doi.org/10.1016/j.paerosci.2014.03.002.

Garcia, J., Gonzalez, D., Rodriguez, A., Santamaria, B., Estremera, J., & Armendia, M. (2019). Application of Impedance Control in Robotic Manipulators for Spacecraft On-orbit Servicing. 2019 24th IEEE International Conference on Emerging Technologies and Factory Automation (ETFA), 836–842. https://doi.org/10.1109/ETFA.2019.8869069.

Garcia, J., Rodriguez, A., Estremera, J., Santamaria, B., Gonzalez, D., & Armendia, M. (2020). Visual Servoing and Impedance Control in Robotic Manipulators for On-Orbit Servicing. 2020 25th IEEE International Conference on Emerging Technologies and Factory Automation (ETFA), 1, 734–741. https://doi.org/10.1109/ETFA46521.2020.9211989.

Ma, G., Jiang, Z., Li, H., Gao, J., Yu, Z., Chen, X., Liu, Y.-H., & Huang, Q. (2015). Hand-eye servo and impedance control for manipulator arm to capture target satellite safely. Robotica, 33(4), 848–864. https://doi.org/10.1017/S0263574714000587.

Mitros, Z., Rekleitis, G., & Papadopoulos, E. (2017). Impedance control design for on-orbit docking using an analytical and experimental approach".

Moghaddam, B. M., & Chhabra, R. (2021). On the guidance, navigation and control of in-orbit space robotic missions: A survey and prospective vision. Acta Astronautica, 184, 70–100. https://doi.org/10.1016/j.actaastro.2021.03.029.

Nocerino, A., Opromolla, R., Fasano, G., & Grassi, M. (2021). LIDAR-based multi-step approach for relative state and inertia parameters determination of an uncooperative target. Acta Astronautica, 181, 662–678. https://doi.org/10.1016/j.actaastro.2021.02.019.

Palmerini, G. B. (2016). Relative navigation in autonomous spacecraft formations. 2016 IEEE Aerospace Conference, 1–10. https://doi.org/10.1109/AERO.2016.7500944.

Peng, J., Xu, W., Liu, T., Yuan, H., & Liang, B. (2021). End-effector pose and arm-shape synchronous planning methods of a hyper-redundant manipulator for spacecraft repairing. Mechanism and Machine Theory, 155, 104062–. https://doi.org/10.1016/j.mechmachtheory.2020.104062.

Pisculli, A., Felicetti, L., Gasbarri, P., Palmerini, G. ., & Sabatini, M. (2014). A reaction-null/Jacobian transpose control strategy with gravity gradient compensation for on-orbit space manipulators. Aerospace Science and Technology, 38, 30–40. https://doi.org/10.1016/j.ast.2014.07.012.

Pomares, J., Felicetti, L., Pérez, J., & Emami, M. R. (2018). Concurrent image-based visual servoing with adaptive zooming for non-cooperative rendezvous maneuvers. Advances in Space Research, 61(3), 862–878. https://doi.org/10.1016/j.asr.2017.10.054.

Pomares, J., Jara, C. A., Pérez, J., & Torres, F. (2015). Direct visual servoing framework based on optimal control for redundant joint structures. International Journal of Precision Engineering and Manufacturing, 16(2), 267–274. https://doi.org/10.1007/s12541-015-0035-z.

Tommasino D., Cipriani G., Doria A., Rosati G. (2020) Effect of End-Effector Compliance on Collisions in Robotic Teleoperation. Applied Sciences. 10(24), 9077. https://doi.org/10.3390/app10249077.

Wang, H., Guo, D., Xu, H., Chen, W., Liu, T., & Leang, K. K. (2017). Eye-in-hand tracking control of a free-floating space manipulator. IEEE transactions on aerospace and electronic systems, 53(4), 1855-1865.

Xu, R., Luo, J., & Wang, M. (2020). Kinematic and dynamic manipulability analysis for free-floating space robots with closed chain constraints. Robotics and Autonomous Systems, 130, 103548–. https://doi.org/10.1016/j.robot.2020.103548.



https://dspace.org/

On-orbit free-floating manipulation using a two-arm robotic system

Ramón, José Luis; Pomares, Jorge; Felicetti, Leonard

2021-10-27
SciTePress - Science and Technology Publications
https://www.insticc.org/node/TechnicalProgram/ROBOVIS/2021/presentationDetails/107121
Ramon JL, Pomares J, Felicetti L. (2021) On-orbit free-floating manipulation using a two-arm robotic system. In: ROBOVIS 2021: 2nd International Conference on Robotics, Computer Vision and Intelligent Systems, 27-28 October 2021, Virtual Event

Downloaded from a DSpace repository. https://dspace.org/